Histidine 55 of Tryptophan 2,3-Dioxygenase Is Not an Active Site Base but Regulates Catalysis by Controlling Substrate Binding‡

Sarah J. Thackray,§ Chiara Bruckmann,§ J. L. Ross Anderson,§ Laura P. Campbell,§ Rong Xiao,|| Li Zhao,|| Christopher G. Mowat,§ Farhad Forouhar,⊥ Liang Tong,⊥ and Stephen K. Chapman*,§

EaStCHEM, School of Chemistry, University of Edinburgh, West Mains Road, Edinburgh EH9 3JJ, U.K., Department of Biological Sciences, Northeast Structural Genomics Consortium, Columbia University, New York, New York 10027, and Center for Advance Biotechnology and Medicine, Rutgers University, Piscataway, New Jersey 08854

Received June 27, 2008; Revised Manuscript Received August 6, 2008

ABSTRACT: Tryptophan 2,3-dioxygenase (TDO) from *Xanthomonas campestris* is a highly specific heme-containing enzyme from a small family of homologous enzymes, which includes indoleamine 2,3-dioxygenase (IDO). The structure of wild type (WT TDO) in the catalytically active, ferrous (Fe^{2+}) form and in complex with its substrate L-tryptophan (L-Trp) was recently reported [Forouhar et al. (2007) *Proc. Natl. Acad. Sci. U.S.A. 104*, 473−478] and revealed that histidine 55 hydrogen bonds to L-Trp, precisely positioning it in the active site and implicating it as a possible active site base. In this study the substitution of the active site residue histidine 55 by alanine and serine (H55A and H55S) provides insight into the molecular mechanism used by the enzyme to control substrate binding. We report the crystal structure of the H55A and H55S mutant forms at 2.15 and 1.90 Å resolution, respectively, in binary complexes with L-Trp. These structural data, in conjunction with potentiometric and kinetic studies on both mutants, reveal that histidine 55 is not essential for turnover but greatly disfavors the mechanistically unproductive binding of L-Trp to the oxidized enzyme allowing control of catalysis. This is demonstrated by the difference in the K_d values for L-Trp binding to the two oxidation states of wild-type TDO (3.8 mM oxidized, 4.1 μM reduced), H55A TDO (11.8 μM oxidized, 3.7 μM reduced), and H55S TDO (18.4 μM oxidized, 5.3 μM reduced).

Oxidative cleavage of the L-tryptophan (L-Trp)[1] pyrrole ring and the insertion of molecular oxygen to produce *N*-formylkynurenine is the first and rate-limiting step in the kynurenine pathway and is catalyzed by tryptophan 2,3-dioxygenase (TDO) and indoleamine 2,3-dioxygenase (IDO) (*2, 3*). The kynurenine pathway processes 95% of L-Trp utilized by humans, leading ultimately to the formation of nicotinamide adenine dinucleotide (NAD^+), an essential coenzyme (*4*). Kynurenine pathway metabolites have been implicated in a number of diseases ranging from neurological disorders, such as cerebral malaria and multiple sclerosis, to cataract formation (*5, 6*). Recent findings have implicated tryptophan catabolism via the kynurenine pathway in immune tolerance, including immune suppression in maternal fetal tolerance and the immune escape of cancers (*7*−*10*). These properties make elucidation of the precise catalytic mechanism of these enzymes extremely important.

TDO and IDO belong to a little-characterized family of dioxygenases that occurs in both prokaryotes and eukaryotes (*11*). These enzymes have homologous 3-D structures but dissimilar primary structures, with sequence identity often less than 10% between family members (*12*). First identified in 1936 (*13*), TDO is mainly found in the liver of mammals but has also been recently identified in mammalian mucous membranes, epididymis, and brain (*14, 15*). The enzyme discussed here is a prokaryotic TDO from *Xanthomonas campestris* (the causative agent of black rot in cabbages), which shares 34% sequence identity with human TDO. The enzyme is a homotetramer that displays high substrate specificity, catalyzing the oxidation of L-Trp, 5-F-Trp, and 6-F-Trp (*1*). In contrast, IDO is found throughout the body in mammals, except for in the liver, and no prokaryotic IDO protein has yet been identified. IDO is monomeric and catalyzes the dioxygenation of L-Trp, D-Trp, serotonin, tryptamine, and 5-OH-Trp, displaying less substrate specificity than TDO (*11, 16*). The crystal structures of WT *X. campestris* TDO (*1, 17*) and human IDO (*12*) have been published recently, revealing similarities between the two enzymes and allowing the identification of potentially important active site residues.

The catalytic mechanisms employed by TDO and IDO have, as yet, not been elucidated, but two proposed mechanisms for tryptophan dioxygenation are shown in Figure 1.

‡ The atomic coordinates for H55A and H55S mutant enzymes of TDO have been deposited in the Protein Data Bank, entries 3BK9 and 3E08, respectively.

* To whom correspondence should be addressed. E-mail: S.K.Chapman@ed.ac.uk. Tel: +44 131 650 4760. Fax: +44 131 650 6453.

§ University of Edinburgh.

|| Rutgers University.

⊥ Columbia University.

[1] Abbreviations: TDO, tryptophan 2,3-dioxygenase; IDO, indoleamine 2,3-dioxygenase; L-Trp, L-tryptophan; 5-F-Trp, 5-fluoro-DL-tryptophan; 6-F-Trp, 6-fluoro-DL-tryptophan; WT, wild type; H55A, histidine 55 → alanine; H55S, histidine 55 → serine; SHE, standard hydrogen electrode; OTTLE, optically transparent thin-layer electrochemistry.

10.1021/bi801202a CCC: $40.75
Published on Web 09/11/2008

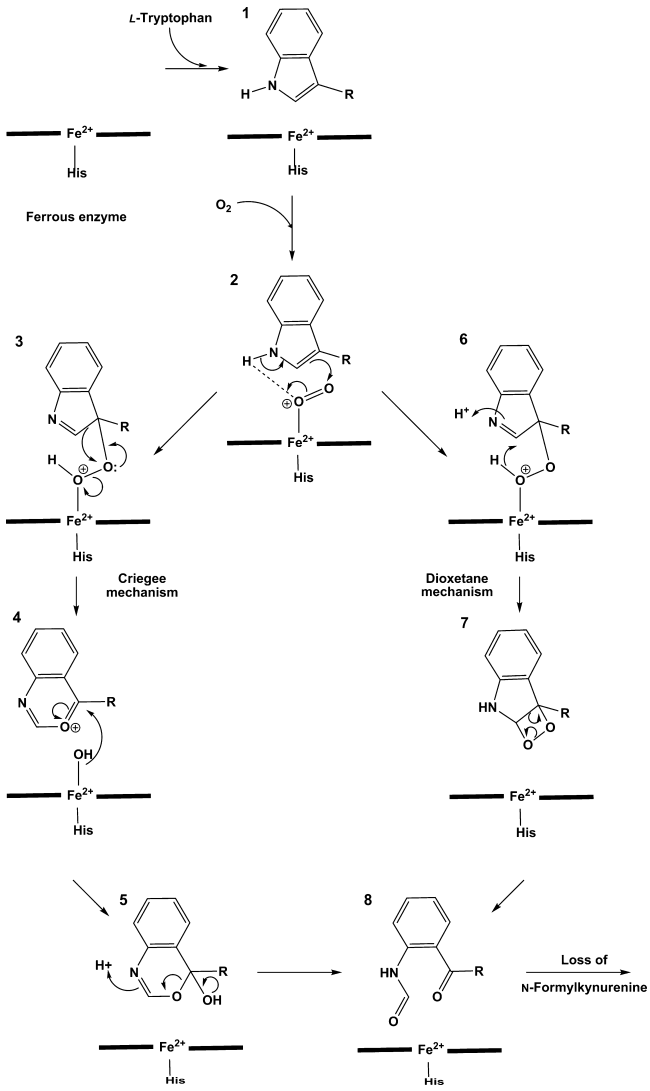

FIGURE 1: Catalytic mechanism proposed for L-tryptophan dioxygenation by TDO. The figure displays an ionic, base-catalyzed mechanism of L-Trp dioxygenation. The first substrate binds to the protein (1), followed by dioxygen binding to form the ternary complex (2). The mechanism proceeds by the formation of a hydroperoxide intermediate (3 and 6), which can undergo two different rearrangements to form the product, *N*-formylkynurenine (8), a Criegee rearrangement (4 and 5), or a dioxetane rearrangement (7). The product is then released leaving the protein in the active ferrous state.

It is proposed that the catalytic mechanism involves the base-catalyzed deprotonation of the indole nitrogen of the substrate. However, the structures of TDO and IDO show that while TDO contains a histidine residue in its active site, IDO does not contain any residues in its active site capable of performing base-catalyzed deprotonation. Instead, it has been proposed that proton abstraction is facilitated by a bound dioxygen molecule (Figure 2).

In the TDO active site histidine 55 hydrogen bonds to L-Trp and is implicated as the active site base. In this study we attempt to resolve the question of whether an active site base is necessary for catalytic activity in TDO. To accomplish this, histidine is replaced by alanine or serine (H55A and H55S mutants of TDO). These substitutions were chosen due to the inability of alanine to act as an active site base and the presence in IDO of a serine residue in the analogous position to histidine 55. We report the crystal

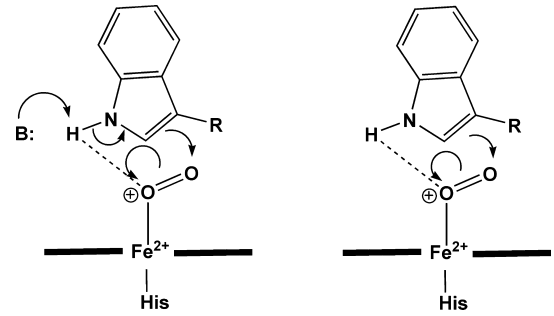

FIGURE 2: Proposed catalytic intermediates involved in proton abstraction of the indole nitrogen of L-tryptophan. The ternary enzyme−substrate−dioxygen complex can either undergo (a) a base-catalyzed proton abstraction or (b) proton abstraction by the bound dioxygen.

structure of the H55A mutant to 2.15 Å resolution and the crystal structure of the H55S mutant to 1.90 Å resolution and relate these to electrochemical and kinetic data for the mutant enzymes.

EXPERIMENTAL PROCEDURES

Genetic Manipulation, Protein Expression, and Purification. Full-length *X. campestris* TDO (NESG (Northeast Structural Genomics Consortium) ID XcR13) was cloned into a pET-21d (Novagen, San Diego, CA) derivative with a C-terminal hexahistidine tag and overexpressed at 17 °C in *Escherichia coli* BL21(DE3) pMGK cells. Point mutations H55A and H55S were created by employing the QuikChange II site-directed mutagenesis kit (Stratagene, La Jolla, CA). Oligonucleotide primers directing mutations were designed in an automated fashion by using the Primer Prim'er program, accessible at www-nmr.cabm.rutgers.edu/bioinformatics/Primer_Primer/. The mutations and their associated ORF were verified by DNA sequence analysis (*1*).

WT TDO and its mutant forms were purified using nickel-affinity and gel-filtration chromatography. Protein and heme concentrations were determined by the Bradford and pyridine hemochrome methods, respectively (*18, 19*). For WT TDO extinction coefficients ε_{404nm} and ε_{431nm} of 180.5 (±0.1) mM^{-1} cm^{-1} and 113.0 (±0.1) mM^{-1} cm^{-1} per protomer were calculated for the ferric and ferrous enzymes, respectively (*1*). For the H55A mutant enzyme extinction coefficients ε_{405nm} and ε_{431nm} were 130.4 (±0.3) mM^{-1} cm^{-1} and 120.0 (±0.1) mM^{-1} cm^{-1} per protomer. For the H55S mutant extinction coefficients ε_{405nm} and ε_{431nm} were 132.0 (±0.3) mM^{-1} cm^{-1} and 116.0 (±0.2) mM^{-1} cm^{-1} per protomer.

Protein Crystallization and Data Collection. Crystallization of H55A and H55S TDO was carried out by hanging drop vapor diffusion at 18 °C in Linbro plates. Crystals were obtained with well solutions comprising 9−10% (w/v) PEG 1000, 80 mM MES buffer, pH 6.3, 20 mM bicine buffer, pH 9.0, 40 mM $MnCl_2$, 400 mM $MgCl_2$, 8−15 mM NaCN, and 20 mM L-Trp. Hanging drops (4 μL volume) were prepared by adding 2 μL of 8 mg mL^{-1} protein (in 50 mM Tris-HCl buffer, pH 8.0, 5 mM in EDTA) to 2 μL of well solution. Red tetragonal shaped crystals appeared after approximately 1 week, reaching full size after 2 weeks. Crystals were immersed in mineral oil prior to being mounted in nylon loops and flash cooled in liquid nitrogen. For crystals of both H55A and H55S enzymes, data sets were collected to a resolution of 2.15 and 1.90 Å, respectively, at station

10.1 at SRS Daresbury (λ = 1.381 Å for H55A TDO, λ = 1.045 Å for H55S). In both cases crystals belonged to space group $P2_1$ with unit cell parameters a = 78.2 Å, b = 117.6 Å, c = 139.3 Å, and β = 95.7 ° (H55A) and a = 77.9 Å, b = 117.8 Å, c = 139.1 Å, and β = 95.7 ° (H55S).

Data processing was carried out using the CCP4 package (*20*) and PHENIX (*21*). The wild-type TDO apoenzyme structure (PDB ID 1YW0), stripped of water, was used as the initial model. Electron density fitting was carried out using PHENIX and Turbofrodo (*22*), and structure refinement was carried out using PHENIX and Refmac (*23*).

Steady-State Kinetic Analysis and Binding Constant Assays. UV−visible spectra were recorded at 25 °C using a Cary 50-Probe UV−visible spectrophotometer. Steady-state turnover assays (at pH 7.5) for oxidation of L-Trp and fluorinated derivatives were performed as described by Ishimura (*24*), except that substrate concentrations of up to 15 mM L-Trp were used. The rate of formation of *N*-formylkynurenine was monitored by measuring the change in absorbance at 321 nm (ϵ_{321}(*N*-formylkynurenine) = 3750 M^{-1} cm^{-1}). Kinetic data were fitted to the Hill equation using Origin software (MicroCal, Northampton, MA). Dissociation constants (K_d) for binding to ferric and ferrous WT TDO and mutant enzymes were determined by established procedures in a Belle Technology anaerobic glovebox with [O_2] maintained below 5 ppm. The electronic absorption spectra at the steady state were recorded by using a stopped-flow spectrophotometer (SX.17MV; Applied-Photophysics, Surrey, U.K.) in conjunction with a diode array detector, housed in an anaerobic glovebox. The oxygen binding affinity (K_m) was measured by standard methods by adding varying concentrations of O_2 ($\leq$1 mM) to the L-Trp saturated (25 mM) assay and by calculating the steady-state parameters as described above. Oxygen concentration was determined spectrophotometrically by titrating aliquots of oxygenated buffer into a solution of electrochemically reduced methyl viologen. The subsequent change in absorbance at 540 nm (ϵ_{540}(methyl viologen) = 13000 M^{-1} cm^{-1}) due to reduction of molecular oxygen was used to calculate [O_2] (*1*).

OTTLE Electrochemistry. Anaerobic potentiometric titrations on WT TDO and mutant enzymes were carried out as previously described (*1, 25*) at 25 °C using a modified quartz EPR OTTLE cell, with the exception that 100 mM Tris-HCl buffer, pH 7.5, and 300 mM KCl (with or without 10% glycerol) buffer was used. A range of mediators were added (2-hydroxy-1,4-naphthoquinone (−145 mV vs SHE), 5-hydroxy-1,4-naphthoquinone (−3 mV), phenazine ethosulfate (+55 mV), phenazine methosulfate (+82 mV), and 1,2-naphthoquinone (+135 mV)) to ensure efficient reduction and reoxidation of the protein. Titrations were performed in both the absence and presence of substrate for WT TDO (15 mM L-Trp), the H55A mutant (5 mM L-Trp), and the H55S mutant (10 mM L-Trp). Heme reduction potentials were determined by fitting the data to a Nernst equation for a single-electron process using Origin software. Reduction potentials are quoted versus the standard hydrogen electrode.

RESULTS AND DISCUSSION

Crystal Structures of H55A and H55S TDO. It was possible to obtain crystals of the ferric H55A and H55S mutant enzymes in binary complex with the substrate due to the much greater affinity of L-Trp for the oxidized mutant enzymes compared to WT TDO (see below and Table 3). For H55A TDO a data set to 2.15 Å resolution was used to refine the structure to a final *R*-factor of 20.5% (R_{free} = 28.5%), while for H55S TDO data to a resolution of 1.90 Å were used to refine the structure to a final *R*-factor of 17.8% (R_{free} = 21.6%). Data collection and refinement statistics are summarized in Table 1.

Table 1: H55A and H55S Data Collection and Refinement Statistics

	H55A	H55S
resolution (Å)	59.66−2.15	17.56−1.90
total no. of reflections	312593	362159
no. of unique reflections	131764	189203
completeness (%)	96.9	93.6
$I/[\sigma(I)]$	9.5	7.3
R_{merge} (%)[a]	10.0	7.8
R_{merge} in outer shell (2.27−2.15 Å) (%)	47.4	48.0
R_{cryst} (%)[b]	20.5	17.8
R_{free} (%)[b]	28.5	21.6
rmsd from ideal values		
bond lengths (Å)	0.022	0.007
bond angles (deg)	2.004	0.952
Ramachandran analysis		
most favored (%)	91.9	92.2
additionally allowed (%)	8.1	7.8
average *B*-factor (overall) (Å^2)	23.2	23.2
average *B*-factor (substrate) (Å^2)	25.7	24.1

[a] $R_{merge} = \sum_h\sum_i|I(h) - I_i(h)|/\sum_h\sum_i I_i(h)$, where $I_i(h)$ and $I(h)$ are the *i*th and mean measurement of reflection *h*, respectively. [b] $R_{cryst} = \sum_h|F_o - F_c|/\sum_h F_o$, where F_o and F_c are the observed and calculated structure factor amplitudes of reflection *h*, respectively. R_{free} is the test reflection data set, 5% selected randomly for cross-validation during crystallographic refinement.

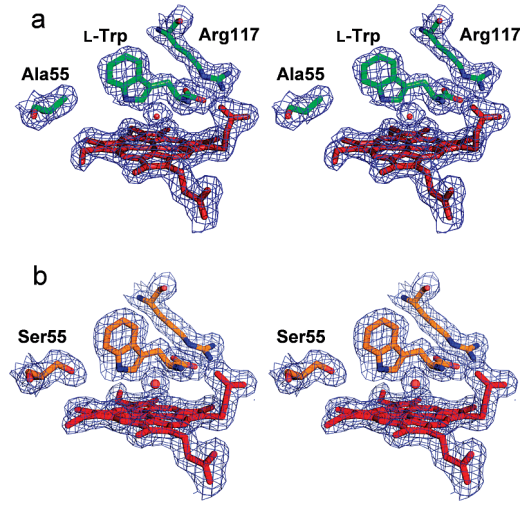

FIGURE 3: Stereoview of electron density around the heme, bound L-Trp, arginine 117, and residue 55 at the active site of (a) H55A TDO and (b) H55S TDO. The electron density map was calculated using Fourier coefficients $2F_o - F_c$, where F_o and F_c are the observed and calculated structure factors, respectively, the latter based on the final model. The contour level is 1σ, where σ is the rms electron density. This figure was generated using PYMOL (*30*).

For each of the H55A and H55S mutant enzymes the final model consists of two TDO tetramers (1 and 2), one of which (tetramer 1) is better defined than the other in the electron density map. The quality of the final electron density map around the active site of chain A of tetramer 1 of both mutant enzymes is shown in Figure 3.

In both mutant enzymes each monomer also binds one heme group and one substrate molecule. Further to this, a

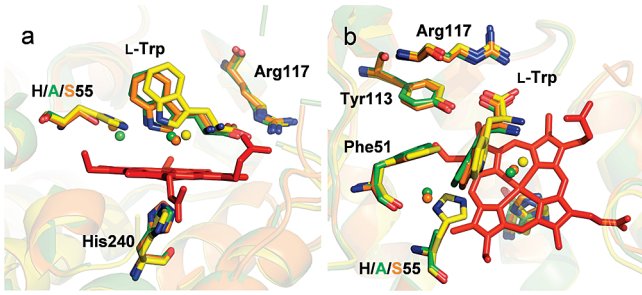

FIGURE 4: An overlay of the active site region of WT TDO (yellow), H55A TDO (green), and H55S TDO (orange) viewed from the side (a) and from above (b). The L-Trp from the H55A and H55S enzymes (in green and orange, respectively) are rotated toward alanine/serine 55 and the heme, relative to the position of the substrate in WT TDO (yellow). The H-bond between histidine 55 and the substrate is lost as a result of the substitution by alanine/serine. The position of the water molecule (water A; see Figure 5) above the heme group in H55A and H55S TDOs is slightly different than in WT enzyme due to the altered substrate binding. This figure was generated using PYMOL (*30*).

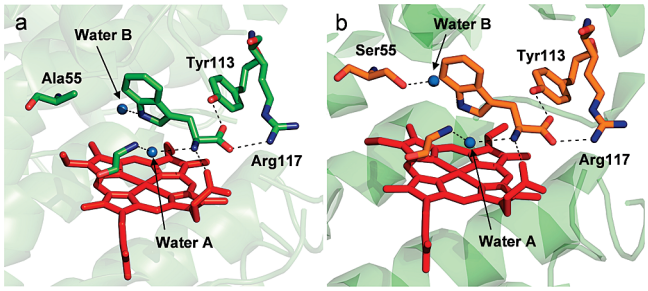

FIGURE 5: The active site of (a) H55A TDO and (b) H55S TDO. Hydrogen-bonding interactions are indicated by dashed lines. The subtly different positions of water B in the mutant enzymes can be seen. This figure was generated using PYMOL (*30*).

second L-Trp molecule is observed at the intersubunit interface close to each of chains A, B, C, D, and E in the H55A TDO structure, and in the H55S model there is one interfacial L-Trp per monomer. In addition, the H55A and H55S models contain 1026 and 1955 water molecules, respectively. The atomic coordinates have been deposited in the Protein Data Bank, accession codes 3BK9 (H55A) and 3E08 (H55S).

Binding Mode of L-Trp to H55A and H55S Mutants. The binding orientation of L-Trp at the active site of the H55A mutant enzyme is slightly different from that observed in the WT TDO structure. An overlay of the active sites of WT TDO and the H55A and H55S enzymes (based on α-C overlay) is shown in Figure 4. The bound L-Trp substrates belonging to the H55A and H55S mutant enzymes (in green and orange, respectively) are shifted toward the side chain of residue 55 relative to the position of L-Trp in the wild-type enzyme (in yellow). Due to the substitution of histidine 55 by alanine or serine the hydrogen-bonding interaction between residue 55 and the substrate indole nitrogen atom is lost. The remaining interactions between the substrate and active site residues that are observed in the wild-type enzyme are maintained in both mutant enzymes (Figure 5).

The active sites of WT TDO and both of the H55A and H55S mutant enzymes contain a water molecule above the distal face of the heme (water A in Figure 5). In all three enzymes this water is H-bonded to the ammonium group of L-Trp and the main-chain amide nitrogen of glycine 125 but is too far (≥2.7 Å) from the heme iron to be a ligand. Further to this, an additional water molecule is found in the active site of the H55A and H55S mutant enzymes (water B in Figure 5) in a position which would be sterically inhibited by the histidine 55 side chain in WT TDO. In the H55A mutant enzyme water B is H-bonded to the substrate indole nitrogen (Figure 5a), but in the H55S model water B is instead H-bonded to the side-chain hydroxyl group of serine 55 (Figure 5b), too far away (~3.4 Å) from L-Trp to maintain a hydrogen-bonding interaction.

In WT TDO the histidine 55 imidazole moiety H-bonds to a water molecule in the substrate-free ferrous state, which is displaced upon binding of substrate. The removal of the histidine side chain in either mutant enzyme would almost certainly result in the absence of a water molecule in such a position.

Steady-State Kinetics and Substrate/Substrate Analogue Binding. It has been previously reported that WT TDO shows catalytic activity toward L-Trp, 6-F-Trp, and 5-F-Trp. We have also observed activity toward 5-methyl-DL-tryptophan and 6-methyl-DL-tryptophan. H55A and H55S mutant enzymes show catalytic activity toward L-Trp, 6-F-Trp, 5-F-Trp, 5-methyl-DL-tryptophan, and 6-methyl-DL-tryptophan but no activity with any other compounds investigated. Kinetic parameters are shown in Table 2, and there is about a 7-fold decrease in k_{cat} values, compared to WT TDO, for both mutant enzymes. As previously reported, there is no inhibition of WT TDO catalytic activity on addition of 1-Me-DL-tryptophan, and the same result is obtained for the mutant enzymes (*1*). This contrasts with findings on IDO, where 1-Me-DL-tryptophan is a known inhibitor of L-Trp dioxygenation activity (*11*). Catalytic activity is observed only by the ferrous enzyme for both WT TDO and its mutant forms, in contrast to recent findings that show catalytic activity by ferric human TDO.

The substitution of histidine 55 may have been expected to render the enzyme inactive if a base is required in the catalytic cycle, but the possibility that a water molecule could be bound, in the vacant space made by the substitution of histidine 55, must be considered. This water molecule could, possibly, act as an active site base dependent on its pK_a in the active site. A water molecule is found near this position in both of the mutant enzymes, but it is not optimally aligned for the deprotonation of L-Trp. It is also located 3.3 Å away from the indole nitrogen atom, outside the range of a normal H-bonding interactions, and we propose that it plays no role in the catalytic cycle (Figure 1). These data, and the relative insensitivity of the WT TDO k_{cat} to pH (Supporting Information Table 1), support the idea that histidine 55 or a solvent molecule is not required to deprotonate the indole nitrogen atom. In IDO where the active site is devoid of solvent, the equivalent residue to histidine 55 is serine 167, which is incapable of acting as a catalytic base. Turnover still occurs, and like TDO k_{cat} is observed to be insensitive to pH (*26*).

The decrease in k_{cat} for L-Trp oxidation in both the H55A and H55S mutants may be explained by the movement of L-Trp in the active site. It can be seen from the crystal structures that for both mutants L-Trp has rotated toward the substituted amino acid (and away from the iron atom) relative to the position of L-Trp in WT TDO. The L-Trp indole ring has also shifted toward the heme (shown in Figure 4). These movements are accompanied by a slight increase in the

Table 2: Kinetic Parameters for *X. campestris* TDO Wild Type and Mutants

	WT TDO			H55A			H55S		
	k_{cat} (s^{-1})	K_m (μM)	k_{cat}/K_m	k_{cat} (s^{-1})	K_m (μM)	k_{cat}/K_m	k_{cat} (s^{-1})	K_m (μM)	k_{cat}/K_m
L-Trp[a]	19.5 ± 1.2	114 ± 1	1.711 (100)	2.86 ± 0.10	133 ± 7	0.215 (100)	2.6 ± 0.01	197 ± 2	0.132 (100)
6-F-D/L-Trp[a]	37.3 ± 0.6	186 ± 12	2.005 (117)	3.78 ± 0.10	195 ± 1	0.194 (90)	3.80 ± 0.04	546 ± 36	0.070 (53)
5-F-D/L-Trp[a]	2.40 ± 0.10	100 ± 6	0.240 (14)	0.68 ± 0.14	194 ± 25	0.035 (16)	0.80 ± 0.01	183 ± 12	0.044 (33)
6-Me-D/L-Trp[a]	41.0 ± 1.2	975 ± 48	0.421 (25)	1.65 ± 0.03	386 ± 4	0.0443 (21)	4.66 ± 0.18	1980 ± 170	0.024 (18)
5-Me-D/L-Trp[a]	3.59 ± 0.05	357 ± 12	0.101 (6)	0.40 ± 0.01	395 ± 20	0.010 (5)	1.45 ± 0.01	1302 ± 21	0.011 (8)

[a] Experiments were performed at 25 °C in 100 mM phosphate buffer, pH 7.5, by varying the concentration of the substrate. It should be noted that these rates are determined under normal atomospheric conditions; therefore, the rates determined are "apparent" for k_{cat} as oxygen is not present at a saturating level. The peak positions of the oxyferrous complex (O_2−TDO) are at 420, 548, and 578 nm, and V_{max}, K_m, and K_i are calculated using L-Trp.

Table 3: Substrate Binding to Oxidized and Reduced *X. campestris* TDO Wild Type and Mutants[a]

	TDO WT (K_d)		H55A (K_d)		H55S (K_d)	
substrate	Fe^{3+} (mM)	Fe^{2+} (μM)	Fe^{3+} (μM)	Fe^{2+} (μM)	Fe^{3+} (μM)	Fe^{2+} (μM)
L-Trp	3.84 ± 0.14	4.1 ± 0.2	11.8 ± 0.2	3.7 ± 1.3	18.4 ± 3.0	5.3 ± 1.0
6-F-D/L-Trp	1.51 ± 0.08	<1.00[b]	165 ± 44	73 ± 3	86 ± 12	6.2 ± 0.9
5-F-D/L-Trp	2.45 ± 0.42	<1.00[b]	67 ± 20	9.0 ± 1.7	73 ± 5	<5.00[b]

[a] Experiments were performed at 25 °C in 100 mM phosphate buffer, pH 7.5. Absorbance changes upon substrate binding are small (~5−10% of initial peak absorbance) but easily quantifiable due to tight substrate binding. [b] Binding was too tight to be measured. Values quoted represent the minimum K_d that can be measured under standard assay conditions.

substrate K_m values, implying a small decrease in the stability of the Michaelis complex. The rotation has resulted in the displacement of the tryptophan indole ring from the dioxygen binding site, thus decreasing overlap of the molecular orbitals involved in catalysis. The transition state for the reaction will be less stable, thus increasing the activation energy for catalysis. This will decrease the turnover rates for both mutants compared to WT TDO.

In WT TDO there is a large increase in the affinity of the enzyme for L-Trp for ferrous vs ferric enzyme ($K_d(Fe^{3+})$ = 3.8 mM, $K_d(Fe^{2+})$ = 4.1 μM) (Table 3). This is in contrast to recent findings for human TDO, where there was found to be little discrimination of binding between the ferric and the ferrous enzymes (*27*). For both mutant proteins this effect is essentially destroyed, with only a small increase shown in the affinity of the ferrous enzyme for L-Trp relative to ferric (Table 3). This trend in K_d is repeated for other substrates. These findings suggest that one role of histidine 55 is to disfavor substrate binding to the oxidized protein, and its removal increases binding affinity by a factor >300. It can therefore be hypothesized that histidine 55 is responsible for controlling the binding affinity of the active site for L-Trp, effectively gating the binding of substrate to WT TDO. In this way histidine 55 greatly disfavors the mechanistically unproductive binding of L-Trp to the oxidized enzyme, promoting the productive binding of L-Trp to the reduced enzyme.

Electrochemical Studies. Electrochemical data for WT TDO and the H55A mutant are shown in Figure 6, and the measured midpoint potentials are displayed in Table 4. There is a much smaller shift in the reduction potential upon binding of substrate ($\Delta E_{mid\ H55A}$ = +23 mV) ($\Delta E_{mid\ H55S}$ = +57 mV) for the mutant enzymes compared to WT TDO ($\Delta E_{mid\ WT}$ = +136 mV). The shift in reduction potential of 23 mV for the H55A mutant enzyme almost perfectly correlates with the increase in affinity for L-Trp for the ferrous vs the ferric form (K_d (Fe(II)) = 3.7 μM vs K_d (Fe(III)) = 11.8 μM), both giving an estimated $\Delta\Delta G$ of 3.5 kJ mol^{-1}. In fact, the difference in these $\Delta\Delta G$ values calculated for WT TDO and the H55A mutant enzyme is approximately 11.5 kJ mol^{-1}, within the range of energies for a single hydrogen bond. The data are less clear for H55S, with a 57 mV shift in the reduction potential on L-Trp binding. The increase in affinity for L-Trp to the ferrous H55S vs the ferric give an estimated $\Delta\Delta G$ of 5.5 kJ mol^{-1}. It is possible that the lower affinity of oxidized WT TDO for substrate may be attributed to subtle changes in the structure of the active site (in terms of the hydrogen-bonding pattern) between the oxidized and reduced enzymes. Binding of L-Trp

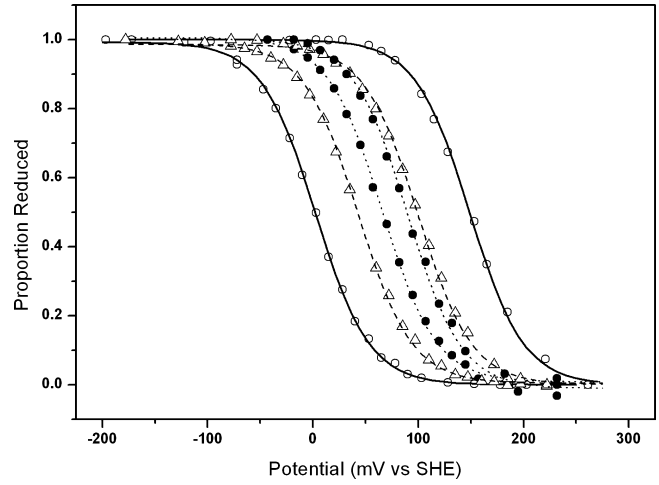

FIGURE 6: OTTLE potentiometric curves for wild-type TDO (open circles), H55A mutant (closed circles), and H55S mutant (open triangles) with (right-hand plots) and without (left-hand plots) L-Trp substrate present (±L-Trp). Each curve is produced from both reduction and oxidation of the layer of interest.

Table 4: Electrochemical Midpoint Potentials

	potential (mV vs SHE)		
	no L-Trp	+L-Trp	change
TDO WT	8 ± 5	144 ± 6	+136
H55A	64 ± 3	87 ± 2	+23
H55S	44 ± 2	101 ± 2	+57
rlTDO[a]	100	160	+60
rhIDO[b]	−30 ± 4	16 ± 3	+46

[a] See ref *29*. [b] See ref *26*.

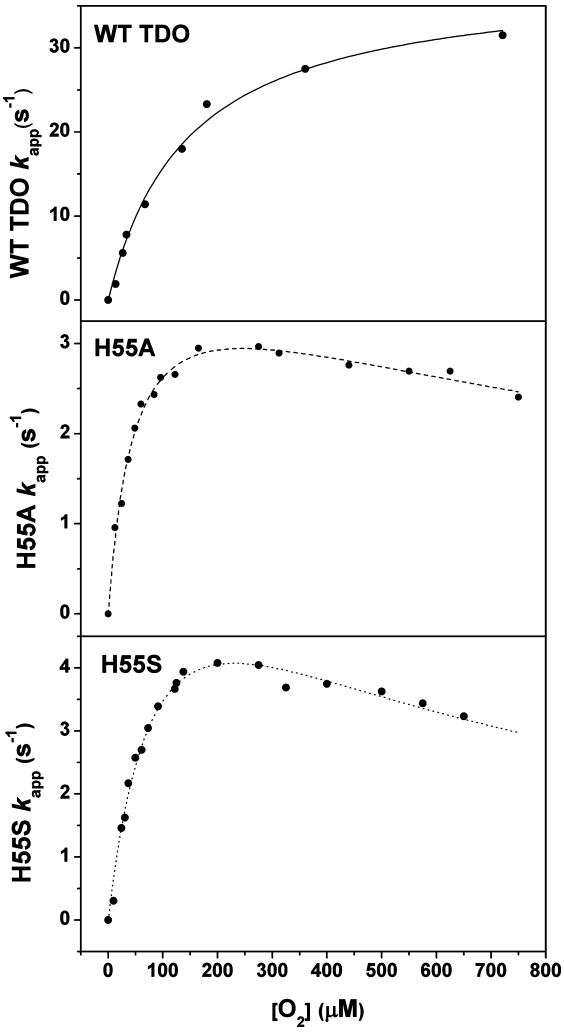

FIGURE 7: Plot of the observed steady-state turnover rate (k_{app}) versus O_2 concentration for wild-type TDO (top) and H55A (middle) and H55S (bottom) mutant forms. The maximum turnover rate (k_{max}), the Michaelis constant (K_m), and the inhibition constant (K_i (for oxygen)) are reported.

accompanies expulsion of solvent from the active site and results in the formation of a hydrogen bond between histidine 55 and the pyrrole nitrogen of the indole L-Trp moiety.

In the H55A mutant enzyme the alanine side chain is unable to form the same hydrogen bonds that histidine 55 can in WT TDO. Consequently, there may be less rearrangement of the active site hydrogen-bonding interactions necessary to allow L-Trp binding, and the K_d for substrate binding to ferric enzyme is correspondingly low. All other amino acid interactions binding L-Trp to the active site are analogous to WT TDO. Consequently, the absence of significant oxidation-state-dependent changes in the active site in H55A TDO results in decreased specificity of binding to the oxidized or reduced enzyme.

The case is similar for the H55S mutant enzyme as the serine side chain is unable to form the same hydrogen bonds that histidine 55 can in WT TDO. It is possible that the serine could form a bonding interaction with a nearby solvent molecule (water 250), but the data suggest that less rearrangement of active site hydrogen-bonding interactions is necessary to allow L-Trp binding than for WT TDO.

Stability of the Michaelis Complex. Figure 7 shows how the observed rate constant for turnover (k_{app}) is dependent on dioxygen concentration, [O_2], under saturating L-Trp concentrations (25 mM). In phosphate buffer (pH 7.5) at 25 °C, $K_m(O_2)$ is approximately 120 μM and k_{app} for WT TDO is only 60% of maximum; however, in the case of the H55A and H55S mutant enzymes, k_{app} is nearly maximal (Table 2). These data seem contrary to the Michaelis model (based on steady-state kinetics) that predicts a lower O_2 binding affinity for the mutant forms.

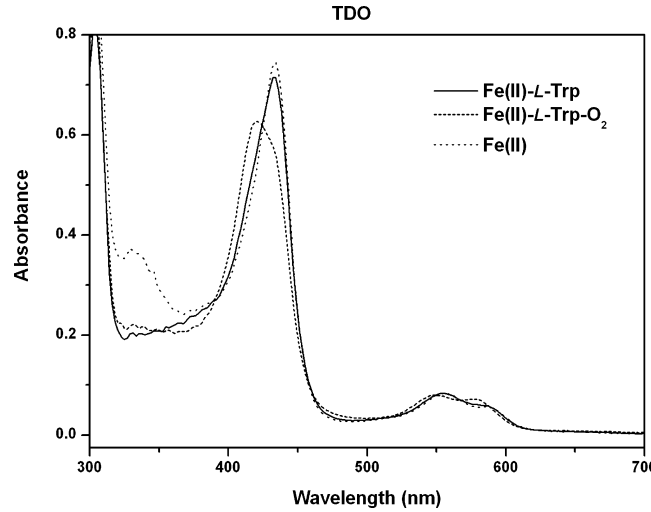

FIGURE 8: Production of the wild-type TDO oxyferrous ternary complex. The peak positions of the oxyferrous ternary complex are at 420, 548, and 578 nm. This decays back to ferrous enzyme and product (*N*-formylkynurenine, peak position 321 nm).

WT TDO has an ordered catalytic cycle in which the reduced enzyme−substrate complex must be formed prior to O_2 binding for turnover to occur (*11, 28*). No ferrous−oxy complex is observed, and addition of oxygen to ferrous WT TDO or the mutant forms in the absence of substrate leads to direct decay to the ferric state. This is also the case for human TDO (*27*), suggesting that instability of the ferrous−oxy species may be common in TDO species. The similar L-Trp binding affinity of the reduced mutant enzymes compared to WT TDO (3.7 and 5.2 μM versus 4.1 μM) and similar K_m values for substrates (Table 2) show that all enzymes can bind substrate and then dioxygen in productive ternary complex formation. Structural data indicate that movement of the indole moiety of L-Trp in the active site is responsible for the decrease in k_{cat} for H55A and H55S. The increased L-Trp binding affinity to the oxidized H55A and H55S enzymes, compared to WT TDO, will lead to a higher probability of nonproductive oxidized enzyme−substrate complex formation, possibly decreasing k_{cat}, but this effect would be small compared to the effect of the destabilized transition state.

Formation and decay of the oxyferrous ternary species generated (Figure 8) for WT TDO show that the (Fe^{2+}−L-Trp) complex displaying a Soret peak at 432 nm binds O_2, producing (Fe^{2+}−L-Trp−O_2), with a corresponding shift in the Soret peak to 419 nm. This then decays to *N*-formylkynurenine (shown by an increase in absorbance at 321 nm) and ferrous enzyme (displaying a Soret peak at 432 nm). This is also observed with 6-F-Trp as the substrate, but for 5-F-Trp some uncoupling is seen, leading to production of the inactive ferric enzyme and the superoxide anion (O_2^-) and release of the substrate. These trends are repeated for H55A and H55S, with uncoupling observed only with 5-F-Trp as substrate. However, the initial

Table 5: Oxygen Dependence of Steady-State Turnover of L-Tryptophan by *X. campestris* TDO Wild Type and Mutants

	TDO WT	H55A	H55S
k_{max} (s^{-1})	35.4 ± 0.9	3.86 ± 0.26	7.88 ± 0.60
K_m (μM)	119 ± 2	45.7 ± 5.6	99 ± 16
K_i (μM)		1380 ± 140	480 ± 50

rates of formation of the ternary complexes are slower, with a rate constant of approximately 50 s^{-1} compared to 100 s^{-1} for WT TDO. Oxyferrous decay parallels this with rate constants of 0.4 s^{-1} and 2 s^{-1} for the mutant enzymes and WT TDO, respectively. This indicates that both mutations do not destabilize the ternary complex significantly, but as the rate of decay is decreased compared to WT TDO, this correlates with a higher activation energy for catalysis due to the movement of the tryptophan indole ring destabilizing the catalytic transition state.

Substrate inhibition is observed at high oxygen concentrations for both mutant forms (Table 5), while none is observed for WT TDO. This unexpected result may be plausibly explained by the lower rate of decay and subsequent slower expulsion of product from the active site by the mutant enzymes. As the active site cavity is larger due to the removal of histidine and its replacement by alanine or serine in the mutant forms, the product, *N*-formylkynurenine, may be less readily expelled at high oxygen concentrations and dioxygen may be able to bind before the product has left. This would trap the product in the active site, causing inhibition of catalytic activity.

CONCLUSIONS

In this study we have investigated whether a putative active site base, histidine 55, is necessary for catalytic activity in TDO. The data we have presented show that in the mutant enzymes H55A and H55S turnover still occurs. This indicates clearly that histidine 55 is not an essential base. Instead, a different role for histidine 55 in controlling substrate binding at the active site has been revealed. On the basis of structural, kinetic, and electrochemical data we have proposed that the role of histidine 55 is to prevent the formation of the nonproductive ferric enzyme−substrate complex. This is most likely achieved by histidine 55 controlling the water content of the substrate-free active site.

SUPPORTING INFORMATION AVAILABLE

A table presenting data on the pH dependence of L-Trp dioxygenation by wild-type TDO and the H55A and H55S mutant forms of the enzyme. This material is available free of charge via the Internet at http://pubs.acs.org.

REFERENCES

1. Forouhar, F., Anderson, J. L. R., Mowat, C. G., Vorobiev, S. M., Hussain, A., Abashidze, M., Bruckmann, C., Thackray, S. J., Seetharaman, J., Tucker, T., Xiao, R., Ma, L.-C., Zhao, L., Acton, T. B., Montelione, G. T., Chapman, S. K., and Tong, L. (2007) Molecular insights into substrate recognition and catalysis by tryptophan 2,3-dioxygenase. *Proc. Natl. Acad. Sci. U.S.A. 104*, 473–478.
2. Takikawa, O. (2005) Biochemical and medical aspects of the indoleamine 2,3-dioxygenase-initiated L-tryptophan metabolism. *Biochem. Biophys. Res. Commun. 338*, 12–19.
3. Yamamoto, S., and Hayaishi, O. (1967) Tryptophan pyrrolase of rabbit intestine. D- and L-tryptophan-cleaving enzyme or enzymes. *J. Biol. Chem. 242*, 5260–5266.
4. Botting, N. P. (1995) Chemistry and neurochemistry of the kynurenine pathway of tryptophan metabolism. *Chem. Soc. Rev. 24*, 401–412.
5. Takikawa, O., Truscott, R. J. W., Fukao, M., and Miwa, S. (2003) Age-related nuclear cataract and indoleamine 2,3-dioxygenase-initiated tryptophan metabolism in the human lens. *Adv. Exp. Med. Biol. 527*, 277–285.
6. Sanni, L. A., Thomas, S. R., Tattam, B. N., Moore, D. E., Chaudhri, G., Stocker, R., and Hunt, N. H. (1998) Dramatic changes in oxidative tryptophan metabolism along the kynurenine pathway in experimental cerebral and noncerebral malaria. *Am. J. Pathol. 152*, 611–619.
7. Mellor, A. L., and Munn, D. H. (2001) Extinguishing maternal immune responses during pregnancy: implications for immunosuppression. *Semin. Immunol. 13*, 213–218.
8. Grohmann, U., Fallarino, F., and Puccetti, P. (2003) Tolerance, DCs and tryptophan: much ado about IDO. *Trends Immunol. 24*, 242–248.
9. Munn, D. H., and Mellor, A. L. (2007) Indoleamine 2,3-dioxygenase and tumor-induced tolerance. *J. Clin. Invest. 117*, 1147–1154.
10. Mellor, A. L., and Munn, D. H. (2004) IDO expression by dendritic cells: tolerance and tryptophan catabolism. *Nat. Rev. Immunol. 4*, 762–774.
11. Sono, M., Roach, M. P., Coulter, E. D., and Dawson, J. H. (1996) Heme-containing oxygenases. *Chem. Rev. 96*, 2841–2887.
12. Sugimoto, H., Oda, S., Otsuki, T., Hino, T., Yoshida, T., and Shiro, Y. (2006) Crystal structure of human indoleamine 2,3-dioxygenase: catalytic mechanism of O_2 incorporation by a heme-containing dioxygenase. *Proc. Natl. Acad. Sci. U.S.A. 103*, 2611–2616.
13. Kotake, Y., and Masayama, I. (1936) The intermediary metabolism of tryptophan. XVIII. The mechanism of formation of kynurenine from tryptophan. *Z. Physiol. Chem. 243*, 237–244.
14. Miller, C. L., Llenos, I. C., Dulay, J. R., Barillo, M. M., Yolken, R. H., and Weis, S. (2004) Expression of the kynurenine pathway enzyme tryptophan 2,3-dioxygenase is increased in the frontal cortex of individuals with schizophrenia. *Neurobiol. Dis. 15*, 618–629.
15. Ishiguro, I., Naito, J., Saito, K., and Nagamura, Y. (1993) Skin L-tryptophan-2,3-dioxygenase and rat hair growth. *FEBS Lett. 329*, 178–182.
16. Littlejohn, T. K., Takikawa, O., Truscott, R. J. W., and Walker, M. J. (2003) Asp274 and His346 are essential for heme binding and catalytic function of human indoleamine 2,3-dioxygenase. *J. Biol. Chem. 278*, 29525–29531.
17. Zhang, Y., Kang, S. A., Mukherjee, T., Bale, S., Crane, B. R., Begley, T. P., and Ealick, S. E. (2007) Crystal structure and mechanism of tryptophan 2,3-dioxygenase, a heme enzyme involved in tryptophan catabolism and in quinolinate biosynthesis. *Biochemistry 46*, 145–155.
18. Bradford, M. M. (1976) A rapid and sensitive method for the quantitation of microgram quantities of protein utilizing the principle of protein-dye binding. *Anal. Biochem. 72*, 248–254.
19. Berry, E. A., and Trumpower, B. L. (1987) Simultaneous determination of hemes *a*, *b*, and *c* from pyridine hemochrome spectra. *Anal. Biochem. 161*, 1–15.
20. Collaborative Computational Project, Number 4. (1994) The CCP4 suite: programs for protein crystallography. *Acta Crystallogr. D50*, 760–763.
21. Adams, P. D., Grosse-Kunstleve, R. W., Hung, L.-W., Ioerger, T. R., McCoy, A. J., Moriarty, N. W., Read, R. J., Sacchettini, J. C., Sauter, N. K., and Terwilliger, T. C. (2002) PHENIX: building new software for automated crystallographic structure determination. *Acta Crystallogr. D58*, 1948–1954.
22. Roussel, A., and Cambillau, C. (1991) TURBO-FRODO, in *Silicon Graphics Geometry Partners Directory 86*, Silicon Graphics, Mountain View, CA.
23. Murshudov, G. N., Vagin, A. A., and Dodson, E. J. (1997) Refinement of macromolecular structures by the maximum-likelihood method. *Acta Crystallogr. D53*, 240–255.
24. Ishimura, Y. (1970) L-Tryptophan 2,3-dioxygenase (tryptophan pyrrolase) (*Pseudomonas fluorescens*). *Methods Enzymol. 17*, 429–434.
25. Ost, T. W. B., Clark, J. P., Anderson, J. L. R., Yellowlees, L. J., Daff, S., and Chapman, S. K. (2004) 4-Cyanopyridine, a versatile spectroscopic probe for cytochrome P450 BM3. *J. Biol. Chem. 279*, 48876–48882.
26. Papadopoulou, N. D., Mewies, M., McLean, K. J., Seward, H. E., Svistunenko, D. A., Munro, A. W., and Raven, E. L. (2005) Redox

and spectroscopic properties of human indoleamine 2,3-dioxygenase and a His303Ala variant: Implications for catalysis. *Biochemistry 44*, 14318–14328.

27. Basran, J., Rafice, S. A., Chauhan, N., Efimov, I., Cheesman, M. R., Ghamsari, L., and Raven, E. L. (2008) A kinetic, spectroscopic, and redox study of human tryptophan 2,3-dioxygenase. *Biochemistry 47*, 4752–4760.

28. Ishimura, Y., Nozaki, M., Hayaishi, O., Nakamura, T., Tamura, M., and Yamazaki, I. (1970) The oxygenated form of L-tryptophan 2,3-dioxygenase as reaction intermediate. *J. Biol. Chem. 245*, 3593–3602.

29. Makino, R., Sakaguchi, K., Iizuka, T., and Ishimura, Y. (1980) L-Tryptophan 2,3-dioxygenase; structure, function and interaction with substrate. *Dev. Biochem. 16*, 179–187.

30. DeLano, W. L. (2002) The PyMOL molecular graphics system, DeLano Scientific, Palo Alto, CA.

BI801202A